Dalton Transactions

Cite this: *Dalton Trans.*, 2012, **41**, 5401

www.rsc.org/dalton

PAPER

Rhodium pyrazolate complexes as potential CVD precursors†

Joseph H. Rivers, Lauren J. DePue Anderson, Cotton M. N. Starr and Richard A. Jones*

Received 20th December 2011, Accepted 9th February 2012
DOI: 10.1039/c2dt12450e

Reaction of 3,5-$(CF_3)_2$PzLi with $[Rh(\mu\text{-}Cl)(\eta^2\text{-}C_2H_4)_2]_2$ or $[Rh(\mu\text{-}Cl)(PMe_3)_2]_2$ in Et_2O gave the dinuclear complexes $[Rh(\eta^2\text{-}C_2H_4)_2(\mu\text{-}3,5\text{-}(CF_3)_2\text{-}Pz)]_2$ (**1**) and $[Rh_2(\mu\text{-}Cl)(\mu\text{-}3,5\text{-}(CF_3)_2\text{-}Pz)(PMe_3)_4]$ (**2**) respectively (3,5-$(CF_3)_2$Pz = bis-trifluoromethyl pyrazolate). Reaction of PMe_3 with $[Rh(COD)(\mu\text{-}3,5\text{-}(CF_3)_2\text{-}Pz)]_2$ in toluene gave $[Rh(3,5\text{-}(CF_3)_2\text{-}Pz)(PMe_3)_3]$ (**3**). Reaction of **1** and **3** in toluene (1 : 4) gave moderate yields of the dinuclear complex $[Rh(PMe_3)_2(\mu\text{-}3,5\text{-}(CF_3)_2\text{-}Pz)]_2$ (**4**). Reaction of 3,5-$(CF_3)_2$PzLi with $[Rh(PMe_3)_4]Cl$ in Et_2O gave the ionic complex $[Rh(PMe_3)_4][3,5\text{-}(CF_3)_2\text{-}Pz]$ (**5**). Two of the complexes, **1** and **3**, were studied for use as CVD precursors. Polycrystalline thin films of rhodium (fcc-Rh) and metastable–amorphous films of rhodium phosphide (Rh_2P) were grown from **1** and **3** respectively at 170 and 130 °C, 0.3 mmHg in a hot wall reactor using Ar as the carrier gas (5 cc min^{-1}). Thin films of amorphous rhodium and rhodium phosphide (Rh_2P) were grown from **1** and **3** at 170 and 130 °C respectively at 0.3 mmHg in a hot wall reactor using H_2 as the carrier gas (7 cc min^{-1}).

Introduction

The use of organometallic complexes for the CVD growth of thin films of noble metals is attractive since mild conditions can often be employed compared to other methods for deposition such as physical vapour deposition (PVD) which requires sophisticated vacuum systems and extreme inputs of heat or energy. CVD processes can also allow for the selective growth of films that have good step coverage compared with traditional techniques such as PVD.[1–3] Thin films of rhodium are used as electrical contacts,[4,5] reflective coatings,[6,7] catalysis,[8,9] and wear-resistant coatings for extreme conditions.[2,10] Previous studies have focused on volatile compounds which feature traditional organometallic ligands such as CO, C_2H_4, C_5H_5, and fluorinated hydrocarbons such as trifluoroacetylacetonate and it has been shown that film quality is dependent on the precursor used.[1,10,11] For example, precursors for the CVD of rhodium films include $[Rh(CO)_2(acac)]$, $[Rh(\mu\text{-}Cl)(CO)_2]_2$, $[(\eta^5\text{-}C_5H_5)Rh(\eta^2\text{-}C_2H_4)_2]$, $[Rh(\eta^3\text{-allyl})_3]$, $[Rh(tfac)_3]$, $[Rh_2(CO)_8]$, and $[(\eta^5\text{-}C_5H_5)Rh(CO)_2]$.[1–3,11] Thin films of Rh and Rh_2O_3 have also been grown by atomic layer deposition (ALD) using organometallic precursors and O_2 as the carrier gas.[12] Film properties are also dependent on substrate type and growth conditions. Impurity levels depend strongly on the precursor and carrier gas used. For example, films grown using argon as a carrier gas using $[Rh(\mu\text{-}Cl)(CO)_2]_2$ at 180 °C contain 49% Rh, 24% C, and 27% O, while films grown under the same conditions from $[Rh(\eta^3\text{-allyl})_3]$ contain 86% Rh and 14% C.[10]

In order to explore the potential to grow films with different compositions and/or new morphologies we have investigated the use of precursors which have non-traditional ligands. New CVD precursors should ideally meet several criteria. The compounds should be volatile at low temperatures (*e.g.* <200 °C), decompose cleanly at a moderately higher temperature, and be readily prepared in high purity and in relatively high yield, especially when precious metal films are desired.[11] In order to impart volatility we have focused our studies on complexes which contain PMe_3, and on ligands that bear CF_3 groups since they are known to give rise to volatile compounds in many cases. Several groups including our own have had success utilizing appropriately substituted pyrazolate ligands to synthesize volatile complexes for use as CVD precursors.[13–15] Using this strategy, we have synthesized a series of new rhodium complexes containing bis-trifluoromethyl pyrazolate (3,5-$(CF_3)_2$-Pz) and PMe_3. The new compounds reported in this paper, $[Rh(\eta^2\text{-}C_2H_4)_2(\mu\text{-}3,5\text{-}(CF_3)_2\text{-}Pz)]_2$ (**1**), $[Rh_2(\mu\text{-}Cl)(\mu\text{-}3,5\text{-}(CF_3)_2\text{-}Pz)(PMe_3)_4]$ (**2**), $[Rh(3,5\text{-}(CF_3)_2\text{-}Pz)(PMe_3)_3]$ (**3**), $[Rh(PMe_3)_2(\mu\text{-}3,5\text{-}(CF_3)_2\text{-}Pz)]_2$ (**4**) and $[Rh(PMe_3)_4][3,5\text{-}(CF_3)_2\text{-}Pz]$ (**5**) were isolated in moderate to good yields, characterized spectroscopically and the solid state structures determined by single crystal X-ray diffraction studies. Preliminary thin film growth studies were performed using **1** and **3**. Using Ar as a carrier gas the precursors gave polycrystalline rhodium and metastable–amorphous rhodium phosphide films respectively. However, using H_2 as the carrier gas the precursors gave only amorphous rhodium and rhodium phosphide films respectively. All films were heavily contaminated with carbon although the use of H_2 as the carrier gas significantly reduced the levels.

Department of Chemistry and Biochemistry, The University of Texas at Austin, 1 University Station A15300, Austin, TX 78712-0165, USA. E-mail: rajones@mail.utexas.edu; Tel: +1 (512) 471-1706

†Electronic supplementary information (ESI) available experimental details of CVD experiments, XPS and XRD data. CCDC 858611–858615. For ESI and crystallographic data in CIF or other electronic format see DOI: 10.1039/c2dt12450e

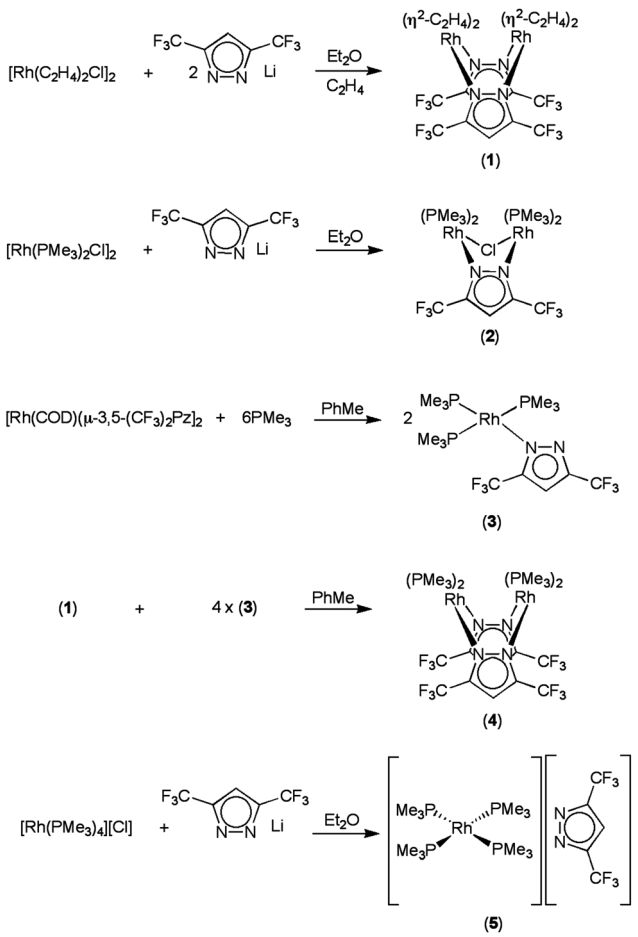

Scheme 1 Synthesis of Rh(I) pyrazolate complexes.

Results and discussion

Synthesis and structures of 1–5

$[Rh(\eta^2\text{-}C_2H_4)_2(\mu\text{-}3,5\text{-}(CF_3)_2\text{-}Pz)]_2$ (1). Reaction of 3,5-$(CF_3)_2$PzLi with $[Rh(\mu\text{-}Cl)(\eta^2\text{-}C_2H_4)_2]_2$ in diethyl ether at −78 °C affords a red solution from which red crystalline $[Rh(\eta^2\text{-}C_2H_4)_2(\mu\text{-}3,5\text{-}(CF_3)_2\text{-}Pz)]_2$ (**1**) can be isolated in high yield (Scheme 1). Improved yields of **1** were obtained when the reaction was conducted under an atmosphere of C_2H_4. The compound crystallizes in the space group $P2_1/c$ with 4 molecules per unit cell. Fig. 1 shows the molecular geometry and atom numbering scheme. Key bond lengths and angles are given in Table 2. Crystallographic details for **1–5** are given in Table 1. The overall molecular structure of **1** is similar to those of the 3,5-dimethylpyrazolate and 3,5-dicarbomethoxypyrazolate analogs $[Rh(\eta^2\text{-}C_2H_4)_2(\mu\text{-}3,5\text{-}(Me)_2Pz)]_2$ and $[Rh(\eta^2\text{-}C_2H_4)_2(\mu\text{-}3,5\text{-}(COOMe)_2Pz]_2$ which have been structurally characterized.[16,17] Thus the Rh_2N_4 core adopts a boat-like configuration with a dihedral angle of 93.4° between pyrazolate rings while the angle between the coordination planes of the Rh centers is 70.8°. The two unique Rh centers in **1** are separated by 3.1160(10) Å which is slightly longer than the distance found in $[Rh(\eta^2\text{-}C_2H_4)_2(\mu\text{-}3,5\text{-}(Me)_2Pz)]_2$ (3.0961(2) Å) but shorter than that in $[Rh(\eta^2\text{-}C_2H_4)_2(\mu\text{-}3,5\text{-}(COOMe)_2Pz]_2$ (3.1937(6) Å). The average Rh–N distance is 2.117(3) Å which compares well with

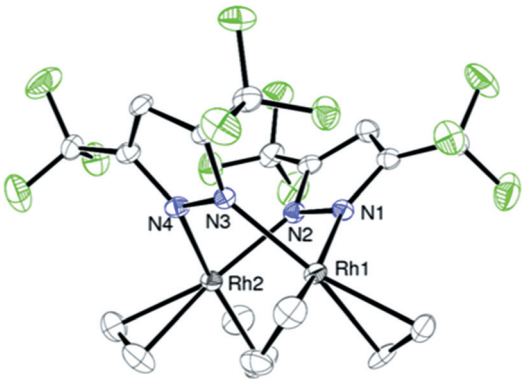

Fig. 1 Molecular structure and atom numbering scheme for $[Rh(\mu\text{-}3,5\text{-}(CF_3)_2Pz)(C_2H_4)_2]_2$ (**1**). Thermal ellipsoids are scaled to the 30% probability level. Hydrogen atoms have been omitted for clarity.

the average Rh–N distance reported for Rh_2 bridged pyrazolate complexes (2.072(2) Å).[18,19] The Rh–C and C=C distances of 2.140(3) Å and 1.363(8) Å fall within normal limits and are similar to average values in other structurally characterized Rh ethylene complexes (2.134(3) Å and 1.386(3) Å respectively).[16,17] The ^{1}H NMR spectrum of **1** in C_6D_6 contains two multiplets at δ 3.22 and 2.97 assigned to two sets of inequivalent olefinic protons. A similar pattern was observed in 1996 by Ciriano, Oro *et al.*[16] whose analysis of variable temperature ^{1}H NMR data is consistent with the rotation of ethylene around the Rh–C_2H_4 bond leading to interconversion of the *trans*-ethylenic protons. A single peak is observed at −58.8 ppm in the ^{19}F NMR spectrum of **1**.

$[Rh_2(\mu\text{-}Cl)(\mu\text{-}3,5\text{-}(CF_3)_2\text{-}Pz)(PMe_3)_4]$ (2). We have also investigated the use of other salt elimination reactions to prepare Rh-3,5-$(CF_3)_2$Pz complexes. Thus, reaction of 3,5-$(CF_3)_2$PzLi with $[RhCl(PMe_3)_2]_2$ in diethyl ether produces the mono-pyrazolate, chloride bridged complex $[Rh_2(\mu\text{-}Cl)(\mu\text{-}3,5\text{-}(CF_3)_2\text{-}Pz)(PMe_3)_4]$ (**2**) which can be recrystallized from hexane at −25 °C as orange needles. Although there are many examples of dinuclear hetero-bridged Rh(III) complexes in the literature, there are fewer Rh_2(I) complexes that are bridged by both a halide and another anionic bridging ligand. Common bridging ligands in combination with halides are thiolates and phosphides as in $[Rh_2(\mu\text{-}Cl)(\mu\text{-}S\text{-}C_6H_6Cl)(CO)_2(P(^tBu)_3)_2]$ and $[Rh_2(\mu\text{-}Cl)(\mu\text{-}P(^tBu)_2)(COD)_2]$.[20,21] There are even fewer halide and pyrazolate bridged dirhodium complexes. For example Trotter and co-workers isolated the chloride/pyrazolate bridged Rh_2 complex, $[Rh_2(\mu\text{-}Cl)(\mu\text{-}Pz)(CO)_4]$ which bears four CO groups.[22] To our knowledge **2** is the first mixed-bridge dinuclear Rh complex that contains bis-trifluoromethyl pyrazolate and PMe_3 ligands. Complex **2** crystallizes in the space group $P2_1/c$ with 4 molecules per unit cell. Fig. 2 shows the overall molecular geometry and atom numbering scheme for **2** and a listing of key bond lengths and angles is given in Table 3. The two crystallographically independent Rh centers have distorted square planar geometries with the central Rh_2N_2Cl core adopting a boat-like conformation. There is more distortion from square planar geometry than that found in $[Rh_2(\mu\text{-}Cl)(\mu\text{-}Pz)(CO)_4]$. For example the *trans* N–Rh–P angles in **2** are 162.71(8) and 170.15(8)° while the analogous

Table 1 Crystallographic data for compounds **1–5**

	1	**2**	**3**	**4**	**5**
Empirical formula	$C_{18}H_{18}F_{12}N_4Rh_2$	$C_{17}H_{37}ClF_6N_2P_4Rh_2$	$C_{14}H_{28}F_6N_2P_3Rh$	$C_{22}H_{38}F_{12}N_4P_4Rh_2$	$C_{17}H_{37}F_6N_2P_4Rh$
Formula weight	724.18	748.64	534.2	916.26	610.28
Temperature (K)	100(2)	123(2)	123(2)	123(2)	123(2)
Space group	$P2_1/c$	$P2_1/c$	$C2$	$P2_1/c$	$P2_1$
Unit cell dimensions					
a (Å)	9.3215(17)	13.489(3)	21.7553(5)	11.0386(3)	9.2999(4)
b (Å)	19.009(3)	10.512(2)	9.3981(2)	15.8199(4)	16.5877(9)
c (Å)	13.182(2)	21.222(4)	12.6181(3)	39.7690(5)	9.4383(4)
α (°)	90	90	90	90	90
β (°)	101.582(5)	104.98(3)	115.627(10)	93.99(2)	111.392(3)
γ (°)	90	90	90	90	90
V (Å^3)	2288.2(7)	2906.9(10)	2326.09(9)	6928.0(3)	1355.68(11)
Z	4	4	4	8	2
D_{calc} (g cm^{-3})	2.102	1.711	1.525	1.757	1.495
Absorption coefficient (mm^{-1})	1.555	1.495	0.988	1.223	0.914
Reflections observed [$I > 2\sigma(I)$]	3069	5138	4439	8327	3452
Final R indices [$I > 2\sigma(I)$][a]	$R_1 = 0.0487$	$R_1 = 0.0364$	$R_1 = 0.0313$	$R_1 = 0.0773$	$R_1 = 0.0663$
	w$R_2 = 0.0915$	w$R_2 = 0.0751$	w$R_2 = 0.0533$	w$R_2 = 0.2079$	w$R_2 = 0.1138$
R indices (all data)[a]	$R_1 = 0.0746$	$R_1 = 0.0543$	$R_1 = 0.0421$	$R_1 = 0.1108$	$R_1 = 0.1572$
	w$R_2 = 0.1002$	w$R_2 = 0.0817$	w$R_2 = 0.0645$	w$R_2 = 0.2219$	w$R_2 = 0.1524$
Absolute structure parameter			−0.04(3)		−0.03(6)
Largest difference peak and hole (e Å^{-3})	0.553 and −0.514	0.778 and −0.633	0.686 and −0.432	2.925 and −0.934	0.757 and −0.856

[a] $R_1 = \Sigma_{hkl}(|F_o| - |F_c|)/\Sigma_{hkl}|F_o|$; $R_2 = [\Sigma w(|F_o| - |F_c|)^2/\Sigma w|F_o|^2]^{1/2}$.

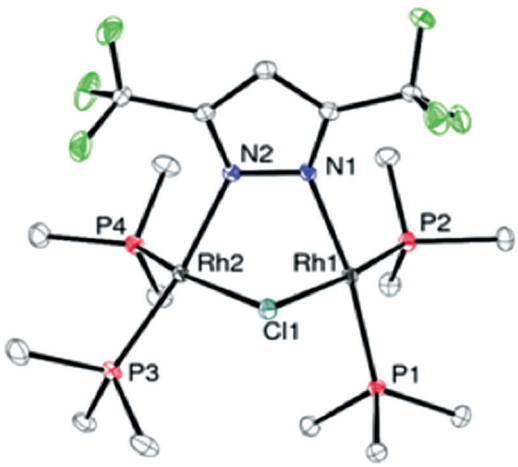

Fig. 2 Molecular structure and atom numbering scheme for [Rh(μ-3,5-$(CF_3)_2$Pz)(μ-Cl)$(PMe_3)_4$] (**2**). Thermal ellipsoids are scaled to the 30% probability level. Hydrogen atoms have been omitted for clarity.

Table 2 Selected bond lengths (Å) and angles (°) for **1**

Bond lengths			
Rh(1)–N(1)	2.117(5)	Rh(2)–C(17)	2.129(7)
Rh(1)–N(3)	2.108(5)	C(11)–C(12)	1.371(9)
Rh(2)–N(2)	2.114(5)	C(13)–C(14)	1.366(10)
Rh(2)–N(4)	2.124(5)	C(15)–C(16)	1.371(11)
Rh(1)–C(11)	2.123(6)	C(17)–C(18)	1.336(10)
Rh(1)–C(12)	2.139(6)	N(3)–Rh(1)–N(1)	83.19(18)
Rh(1)–C(13)	2.151(6)	N(2)–Rh(2)–N(4)	82.66(19)
Rh(1)–C(14)	2.148(6)	C(11)–Rh(1)–C(12)	37.5(2)
Rh(2)–C(15)	2.143(8)	C(14)–Rh(1)–C(13)	37.1(3)
Rh(2)–C(16)	2.141(8)	C(15)–Rh(2)–C(16)	37.3(3)
Rh(2)–C(18)	2.138(7)	C(17)–Rh(2)–C(18)	36.5(3)

Table 3 Selected bond lengths (Å) and angles (°) for **2**

Bond lengths		Bond angles	
Rh(1)–N(1)	2.132(3)	N(1)–Rh(1)–P(2)	95.45(8)
Rh(2)–N(2)	2.120(3)	N(1)–Rh(1)–P(1)	170.15(8)
Rh(1)–Cl(1)	2.4513(10)	P(2)–Rh(1)–P(1)	93.54(4)
Rh(2)–Cl(1)	2.4428(12)	N(1)–Rh(1)–Cl(1)	80.04(8)
Rh(1)–P(1)	2.2252(10)	P(2)–Rh(1)–Cl(1)	174.15(3)
Rh(1)–P(2)	2.1907(10)	P(1)–Rh(1)–Cl(1)	90.72(3)
Rh(2)–P(3)	2.2155(10)	N(2)–Rh(2)–P(4)	95.25(8)
Rh(2)–P(4)	2.1846(12)	N(2)–Rh(2)–P(3)	162.71(8)
P(4)–Rh(2)–Cl(1)	165.85(3)	P(4)–Rh(2)–P(3)	94.37(4)
P(3)–Rh(2)–Cl(1)	93.27(4)	N(2)–Rh(2)–Cl(1)	80.53(8)

value in [Rh_2(μ-Cl)(μ-Pz)$(CO)_4$] is 176.0(2)°. In addition the carbonyl complex displays almost no bending between the edge sharing rhodium–ligand planes (angle between planes 145°) and has a Rh–Rh distance of 3.6275(9) Å whereas **2** has an angle of 100° between planes and a Rh–Rh distance of 3.0503(7) Å. The structural differences are consistent with computational studies by Lledos and Alvarez who postulated that the angle between planes and metal–metal distances in edge-sharing binuclear square planar d^8 complexes are smaller when good σ-donor ligands are present.[23] Steric interactions may also be involved as **2** contains PMe_3 instead of CO as well as the bis(CF_3) substituted pyrazolate instead of unsubstituted Pz in [Rh_2(μ-Cl)(μ-Pz)$(CO)_4$]. Solutions of **2** in C_6D_6 are unstable and there is a slow conversion to a mixture of [Rh(μ-Cl)$(PMe_3)_2]_2$ and **4** which takes place over several days. Thus the ^{31}P-NMR spectra of fresh solutions of **2** in C_6D_6 at room temperature exhibit a complex pattern suggesting a dynamic system involving dissociation of the dinuclear complex in solution. The spectrum consists of four doublets, two of which exhibit Rh–P coupling (J = 167 Hz) while the other two signals are doublets of quartets with both Rh–P and F–P coupling (J = 204 and 4 Hz respectively). The

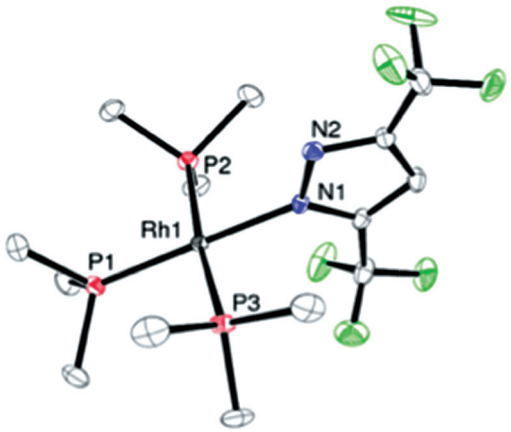

Fig. 3 Molecular structure and atom numbering scheme for [Rh(3,5-$(CF_3)_2$-Pz)$(PMe_3)_3$] (**3**). Thermal ellipsoids are scaled to the 30% probability level. Hydrogen atoms have been omitted for clarity.

^{19}F NMR consists of a doublet (J_{P-F} = 4 Hz). After several days at room temperature the solution changes from bright orange to dark yellow and ^{31}P and ^{19}F NMR spectra reveal the presence of $[Rh(\mu\text{-Cl})(PMe_3)_2]_2$ and **4**.[22] Complex **4** can be isolated from these solutions by cooling aged toluene solutions of **2** to −25 °C.

[Rh(3,5-$(CF_3)_2$-Pz)$(PMe_3)_3$] (3). Treatment of a toluene solution of $[Rh_2(\mu\text{-}3,5\text{-}(CF_3)_2\text{-Pz})(COD)]_2$ with six equivalents of PMe_3 at room temperature affords the neutral monomeric complex Rh(3,5-$(CF_3)_2$-Pz)$(PMe_3)_3$ (**3**) in high yield. The complex can also be prepared by the reaction of $Rh(PMe_3)_3Cl$ with 3,5-$(CF_3)_2$-PzLi and is readily recrystallized from hexane at −25 °C as yellow needles. There are numerous examples of Rh(I) complexes of the type $Rh(PR_3)_3X$, but somewhat surprisingly, to the best of our knowledge, this is the first pyrazolate complex of this kind. The compound crystallizes in the space group *C*2 with four molecules per unit cell. Fig. 3 shows the overall molecular geometry and atom numbering scheme for **3** and a listing of key bond lengths and angles appears in Table 4. The Rh center possess nearly perfect square planar coordination with the mutually *trans* PMe_3 groups coordinated slightly closer to the pyrazolate ligand. The pyrazolate ring is oriented perpendicular to the Rh coordination plane. Interestingly the molecule has near molecular mirror symmetry yet does not adopt mirror symmetry that could be imparted crystallographically. The Rh–P bond *trans* to the pyrazolate is shorter (2.228(1) Å) than the mutually *trans* Rh–P bonds (avg. 2.3125(7) Å) by 0.0845(12) Å. The same contraction in Rh–P bonds *trans* to the "X" ligand are found in $Rh(PMe_3)_3Cl$, $Rh(PMe_3)_3(S\text{-}C_6H_5)$, and $Rh(PMe_3)_3(O\text{-}p\text{Tol})$ where the Rh–P distance is shorter than the mutually *trans* Rh–PMe_3 distance by 0.095(1) Å, 0.063(3) Å, and 0.1058(11) Å respectively.[24–26] This observation is likely due to the π-basic nature of these anionic ligands resulting in extra electron density available at the metal to overlap in a π fashion with PMe_3. In contrast the mutually *trans* PMe_3 ligands compete with each other to accept electron density for π-bonding. The ^{31}P NMR spectrum of **3** contains a well resolved doublet of triplets centered at −0.51 ppm (J_{P-Rh} = 154.1 Hz, J_{P-P} = 47.3 Hz) assigned to P *trans* to pyrazolate. There is also a doublet of doublets centered at −10.21 ppm (J_{P-Rh} = 135.0 Hz, J_{P-P} = 46.5 Hz). The ^{19}F NMR spectrum contains two singlets at −58.5 and −60.0 ppm assigned to the two inequivalent CF_3 groups. The complex is stable in solution under an inert atmosphere, but quickly decomposes in the presence of air in solution and the solid state at room temperature.

Table 4 Selected bond lengths (Å) and angles (°) for **3**

Bond lengths		Bond angles	
Rh(1)–N(1)	2.096(3)	N(1)–Rh(1)–P(1)	179.31(10)
Rh(1)–P(1)	2.2278(11)	N(1)–Rh(1)–P(2)	87.33(9)
Rh(1)–P(2)	2.3140(11)	N(1)–Rh(1)–P(3)	86.22(9)
Rh(1)–P(3)	2.3111(11)	P(1)–Rh(1)–P(2)	92.62(4)
		P(1)–Rh(1)–P(3)	93.88(4)
		P(3)–Rh(1)–P(2)	172.62(4)

$[Rh_2(\mu\text{-}3,5\text{-}(CF_3)_2\text{-Pz})(PMe_3)_2]_2$ (4). During the course of this work we isolated and characterized the symmetrical tetra phosphine Rh_2 bis-pyrazolate complex $[Rh_2(\mu\text{-}3,5\text{-}(CF_3)_2\text{-Pz})(PMe_3)_2]_2$ (**4**) in low yields from a number of reactions. For example, reaction of $[Rh(\mu\text{-Cl})(PMe_3)_2]_2$ with two equivalents of 3,5-$(CF_3)_2$PzLi produces low yields of a mixture of **2** and **4**. As noted above **4** can also be isolated from aged solutions of **2** in toluene while reaction of **1** with excess PMe_3 produces only the mononuclear complex **3**. A reliable route to **4** in moderate yield (34%) was discovered by simply combining a mixture of **1** and **3** in toluene in a 1 : 4 mole ratio and slowly purging the solution with a stream of N_2 to remove C_2H_4. Subsequent removal of solvent and cooling (−25 °C) produces **3** as yellow crystals. There are many examples of bis-pyrazolate bridged Rh_2(I) complexes of formula $[Rh(Pz)L_2]_2$ where L is a neutral ligand. Most examples contain olefinic ligands, as in **1**, $[Rh(COD)_2(\mu\text{-}3,5\text{-}(Me)_2Pz)]_2$, $[Rh(\eta^2\text{-}C_2H_4)_2(\mu\text{-}3,5\text{-}(Me)_2Pz)]_2$, and $[Rh(\eta^2\text{-}C_2H_4)_2(\mu\text{-}3,5\text{-}(Me)_2Pz)]_2$. Examples with carbon monoxide and isocyanides include $[Rh(\mu\text{-}3,5\text{-}(Me)_2\text{-Pz})(CO)_2]_2$, $[Rh(\mu\text{-Pz})(CO)_2]_2$, and $[Rh(\mu\text{-Pz})(CNBu^t)_2]_2$.[12,16,27] To the best of our knowledge **4** is the first structurally characterized bis-pyrazolate complex of this type utilizing a trialkylphosphine exclusively as the neutral ligand. Complex **4** crystallizes in the space group $P2_1/c$. There are two crystallographically independent, yet chemically identical, molecules in the asymmetric unit with a total of 8 molecules per unit cell. Fig. 4 shows the overall molecular geometry and atom numbering scheme for **4** and a listing of key bond lengths and angles appears in Table 5.

The molecular geometry of **4** is similar to that of **1** with the Rh_2N_2 core adopting a boat-like conformation with a dihedral angle of 80.1° between pyrazolate rings and the angle between the two Rh(I) coordination planes of 70.1°. This conformation results in a Rh–Rh distance of 3.1220(7) Å which is longer than the analogous distance found in **1**, no doubt due to the relatively bulkier PMe_3 ligands. The average Rh–N distance (2.144(3) Å) is slightly longer than the average Rh–N distance found in bridging pyrazolate complexes (2.072(2) Å).[13] The average Rh–P distance (2.2144(10) Å) is also slightly longer than the average Rh–P distance found in $[Rh(\mu\text{-Cl})(PMe_3)_2]_2$ (2.1948(9) Å). Again the steric requirements of the CF_3 substituted pyrazolate and PMe_3 ligands are possible causes for these slightly longer than average bond lengths. The ^{31}P NMR spectrum of **4** contains

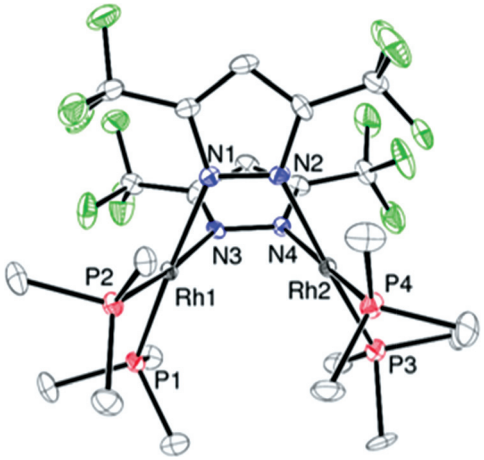

Fig. 4 Molecular structure and atom numbering scheme for one of the crystallographically independent molecules of [Rh(μ-3,5-$(CF_3)_2$Pz)-$(PMe_3)_2]_2$ (**4**). Thermal ellipsoids are scaled to the 30% probability level. Hydrogen atoms have been omitted for clarity.

Table 5 Selected bond lengths (Å) and angles (°) for **4**

Bond lengths		Bond angles	
Rh(1)–N(1)	2.129(9)	N(3)–Rh(1)–P(1)	93.5(2)
Rh(1)–N(3)	2.142(8)	N(1)–Rh(1)–P(2)	93.0(2)
Rh(1)–P(1)	2.211(3)	N(3)–Rh(1)–P(2)	173.1(2)
Rh(1)–P(2)	2.212(3)	P(1)–Rh(1)–P(2)	92.43(12)
Rh(2)–N(4)	2.134(9)	N(4)–Rh(2)–N(2)	80.2(3)
Rh(2)–N(2)	2.153(9)	N(4)–Rh(2)–P(3)	93.5(2)
Rh(2)–P(4)	2.211(3)	N(2)–Rh(2)–P(3)	172.9(3)
Rh(2)–P(3)	2.224(3)	N(4)–Rh(2)–P(4)	172.9(3)
N(1)–Rh(1)–N(3)	81.2(3)	N(2)–Rh(2)–P(4)	92.9(3)
N(1)–Rh(1)–P(1)	174.5(2)	P(4)–Rh(2)–P(3)	93.44(13)

a doublet centered at 1.62 ppm (J_{Rh-P} = 172.5 Hz), and the ^{19}F NMR spectrum contains only a singlet at −57.97 ppm. These observations suggest that there is no dissociation of the dimer in solution.

[Rh(PMe$_3$)$_4$][(3,5-(CF$_3$)$_2$-Pz)] (5). Reaction of [Rh(PMe$_3$)$_4$][Cl] with one equivalent of 3,5-$(CF_3)_2$-PzLi in diethyl ether in the presence of excess PMe_3 affords the ionic compound [Rh-$(PMe_3)_4$][(3,5-$(CF_3)_2$-Pz)] (**5**) in moderate yields. Cationic complexes of the type $[RhL_4]^+$ are known for L = PMe_3, PPh_3, and $P(OR)_3$ and with counter anions such as $[Cl]^-$, $[PF_6]^-$, $[BPh_4]^-$, and $[BH_4]^-$.[24,28–30] We have also recently described the $[B(C_6F_5)_4]^-$ analogue $[Rh(PMe_3)_4][B(C_6F_5)_4]$.[31] Rh(I) complexes of this type provide a coordinative and electronically unsaturated metal center which undergo oxidative-addition reactions of relevance to catalysis. Complex **5** crystallizes in the space group $P2_1$ with 2 molecules in the unit cell. Fig. 5 shows the overall molecular geometry and atom numbering scheme for **5** and a listing of key bond lengths and angles appears in Table 6. The pyrazolate anion is fully dissociated in the solid state with the closest contact between anion and cation of 3.49(2) Å (F(6)–C(16)). The Rh(I) center is nearly square planar with the coordination having a slight "butterfly" or "bow-tie" geometry likely due to steric crowding. Both pairs of *trans* PMe_3 groups are

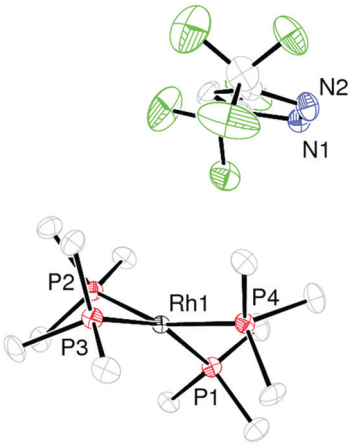

Fig. 5 Molecular structure and atom numbering scheme for [Rh-$(PMe_3)_4$][3,5-$(CF_3)_2$Pz] (**5**). Thermal ellipsoids are scaled to the 30% probability level. Hydrogen atoms have been omitted for clarity.

Table 6 Selected bond lengths (Å) and angles (°) for **5**

Bond lengths		Bond angles	
Rh(1)–P(3)	2.295(3)	P(2)–Rh(1)–P(1)	91.80(9)
Rh(1)–P(2)	2.298(3)	P(3)–Rh(1)–P(1)	157.39(10)
Rh(1)–P(1)	2.299(3)	P(3)–Rh(1)–P(2)	91.57(10)
Rh(1)–P(4)	2.313(2)	P(3)–Rh(1)–P(4)	92.06(9)
P(1)–Rh(1)–P(4)	92.77(10)	P(2)–Rh(1)–P(4)	158.95(10)

bound so that there is a deviation in the P–Rh–P angle from 180° (P(1)–Rh–P(3) 157.39(10)°, P(2)–Rh–P(2) 158.95(10)°). These deviations are not as severe as those found in [Rh-$(PMe_3)_4$][Cl] (P–Rh–P 147.87(3)° av.).[24] The difference is likely due to different packing forces present in the crystals. The average Rh–P distance in **5** is almost identical to that found in [Rh$(PMe_3)_4$][Cl] (2.3013(14) *vs.* 2.2970(7) Å respectively). The CF_3 groups were found to possess some rotational disorder and better refinement was achieved through modeling this on one of the groups. The ^1H NMR spectrum of **5** in C_6D_6 contains a complex multiplet for the PMe_3 hydrogens centered at 0.78 ppm while the $^{31}P\{1H\}$ spectrum is a broad singlet centered at −13.1 ppm. The presence of a single peak at −59.2 ppm in the ^{19}F NMR spectrum is consistent with the complex existing in the ionic form in solution. Conductivity measurements in MeCN are also consistent with **5** existing as a 1 : 1 electrolyte in this solvent.

Film growth and characterization†

Films were deposited in a horizontal hot-wall CVD reactor using high purity Ar or H_2 as the carrier gas. Using Ar as the carrier gas at a deposition temperature of 500 °C for 60 minutes *ca.* 100 mg of precursor **1** gave crystalline rhodium films with thicknesses ranging from 40 to 60 nm (from SEM). The precursor was heated to 170 °C and the lines leading to the deposition chamber were held at 175 °C with a flow rate of 5 sccm and pressure of 0.3 Torr. Deposition temperatures below 400 °C resulted in much of the precursor passing through the deposition

Table 7 Film composition using **1** and **3** and Ar and H_2 as carrier gases

Precursor	Carrier gas	Precursor temperature (°C)	Deposition temperature (°C)	Film composition (%)		
				Rh	C	P
1	Ar	170	500	15.0	78.3	n/a
1	H_2	170	500	58.1	41.9	n/a
3	Ar	130	350	64.0	21.0	15.0
3	H_2	130	350	67.0	15.0	18.0

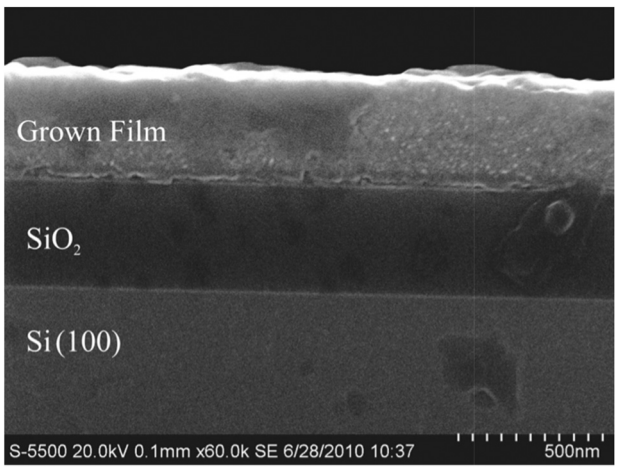

Fig. 6 Side on view of a typical film grown from **3**.

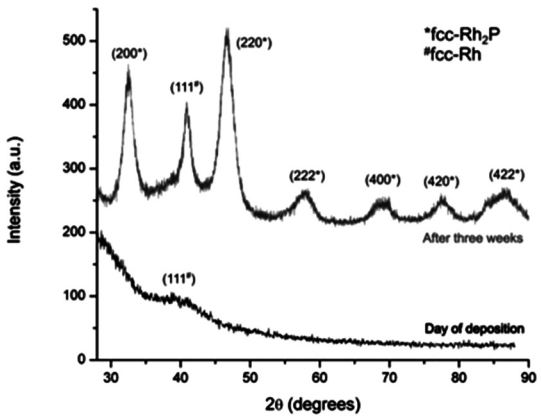

Fig. 7 XRD data: comparison of film grown from **3** at the time of deposition and three weeks later.

chamber intact, while higher temperatures resulted in decomposition of nearly all the precursor. Grazing-incidence XRD revealed only the most intense peaks for fcc-Rh at 40.8° (111) and 47.45° (200) 2θ.[32] XPS analysis revealed mainly Rh, O, and C with traces of F and N on the surface of the film. Sputtering of the film with ionized argon efficiently removed surface contamination and after 60 seconds of sputtering the only detectable elements were Rh and C. The quantification of Rh and C was carried out using the Rh 3d doublet and C 1s peaks. The C 1s peak was always a single, sharp peak, and the Rh 3d doublet did not show any evidence of more than one chemical oxidation state present. After removal of the surface contaminants, the Rh concentration was determined to be 15% with 6.7% nitrogen while carbon comprised the other 78.3%. Further sputtering did not reveal any significant change in concentration within experimental error.

With the exception of the surface contamination, the films were quantitatively homogenous through to the substrate. In the absence of all other impurities save carbon in the bulk material, the relatively high carbon impurities likely come from decomposition of the ethylene at the necessary high deposition temperatures. The metallic silver to pink films were only slightly adhesive to the SiO_2 substrate failing both the scratch and tape tests. Other groups have seen dramatic decreases in carbon impurities when H_2 is used as the carrier gas.[10] Films grown using H_2 as the carrier gas had significantly less carbon as shown in Table 7. After removal of the surface contaminants, the Rh concentration was determined to be 58.1% and carbon 41.9%.

The use of *ca.* 100 mg of precursor **3** with a deposition temperature of 350 °C for 30 minutes resulted in the deposition of amorphous rhodium phosphide (Rh_2P) films with thicknesses of 150–200 nm (from SEM). The precursor was heated to 130 °C and the lines leading to the deposition chamber were held at 140 °C with a flow rate of 5 sccm and pressure of 0.3 Torr. A side on view of a typical film is shown in Fig. 6. Initial grazing-incidence XRD revealed only one weak very broad peak corresponding to the most intense peak for rhodium metal at 40.8° 2θ.[32] XPS analysis revealed mainly Rh, O, P, and C with traces of F and N at the surface of the film. Sputtering of the film with ionized argon efficiently removed surface contamination and after 60 seconds of sputtering the only detectable elements were Rh, P and C. The quantification of Rh, P, and C were carried out using the Rh 3d doublet, P 2p doublet, and C 1s peaks. The C 1s peak was always a single, sharp peak, while the Rh 3d and P 2p doublets did not show any evidence of more than one oxidation state present after the oxide layer was removed. After removal of the surface contaminants, the Rh concentration was determined to be 64% with a P concentration of 15% while carbon comprised the other 21%. Interestingly, after three weeks of standing under atmospheric conditions, subsequent XRD analysis showed strong peaks corresponding to fcc-Rh_2P and fcc-Rh metal.[32,33] A comparison of the two XRD patterns is shown in Fig. 7.

A second amorphous film was grown using H_2 as a carrier gas. After removal of the surface contaminants, the Rh concentration was determined to be 67% with a P concentration of 18% while carbon comprised the other 15%. While a reduction in carbon is achieved by using H_2 as the carrier gas it is not entirely removed as shown in Table 7.

We have recently reported RuP amorphous alloys grown utilizing the ruthenium trimethylphosphine complex, *cis*-$RuH_2(PMe_3)_4$.[34] The incorporation of phosphorous appears to hinder the formation of crystalline Ru and similar effect is

postulated to be taking place here. However, in the case of films grown from **3** at 350 °C the amorphous material crystallizes after several days at room temperature. When deposition temperatures were raised above 400 °C, the films were found to be crystalline immediately after deposition. Annealing of the amorphous films at 350–450 °C under vacuum for several hours also produced mixtures of crystalline fcc-Rh_2P and fcc-Rh. Higher annealing temperatures resulted in a dominance of fcc-Rh with little to no Rh_2P observed by XRD.

Conclusions

The synthesis and characterization of a series of rhodium(I) complexes containing the bis-trifluoromethyl-pyrazolate ligand is described. Two of the complexes, **1** and **3**, were shown to be appropriate for use as CVD precursors. **1** deposits fcc-Rh films at deposition temperatures above 500 °C which are heavily contaminated with carbon. Complex **3** is the first pyrazolate complex of the type $Rh(PMe_3)_3L$, and it was shown to be a viable precursor for the deposition of metastable–amorphous Rh_2P films. The use of H_2 as a carrier gas produced amorphous films with less carbon impurities than films grown using Ar.

Experimental

General procedures

NMR spectra were recorded at room temperature on either a Varian Unity 300 MHz or Inova 500 MHz spectrometer. Melting points were taken on an Electrothermal instrument in sealed capillaries under 1 atmosphere of N_2 or under vacuum at 0.1 Torr N_2. IR spectra were obtained on a Nicolet Avatar 330 FTIR spectrometer with a Smart Performer ATR attachment. Mass spectrometry data was collected on a Thermo LTQ Quantum using electrospray ionization in positive mode. Microanalysis performed by Galbraith Laboratories, Inc. Knoxville, TN. All reactions were performed under a dry, oxygen-free nitrogen atmosphere or under vacuum using standard Schlenk line and dry box techniques. All solvents were dried prior to use by distillation from molten sodium or sodium benzophenone ketyl under nitrogen. 3,5-Bis(trifluoromethyl)pyrazole,[35] $[Rh(PMe_3)_2Cl]_2$,[36] $[Rh(PMe_3)_4]Cl$,[37] $[Rh(COD)(\mu\text{-}3,5\text{-}(CF_3)_2Pz)]_2$, and $[Rh(C_2H_4)_2Cl]_2$[38] were prepared as described in the literature. For the thin film growth studies quantitative elemental characterization was performed using XPS (Kratos AXIS Ultra DLD, monochromatic Al Kα). Further film characterization was performed with scanning electron microscopy (SEM) (Zeiss Supra 40 VP), and grazing-incident (3° incident) X-ray diffraction (XRD) (Bruker-Nonius D8 Advance, Cu Kα).

$[Rh(C_2H_4)_2(\mu\text{-}3,5\text{-}(CF_3)_2Pz)]_2$ (1). A solution of n-BuLi (1.07 ml, 1.6 M) in C_6H_{14} was added to a solution of 3,5-$(CF_3)_2$PzH (0.35 g, 1.72 mmol) in Et_2O (40 ml) at −78 °C. This solution was stirred for 30 minutes and then warmed to room temperature and stirred for 90 minutes. The solution was then cannulated into a solution of $[Rh(C_2H_4)_2Cl]_2$ (0.334 g, 0.86 mmol) under an atmosphere on C_2H_4 at −78 °C. The solution was then warmed slowly to room temperature and stirred overnight forming a white precipitate and a bright red solution. The solution was filtered through a short bed of Celite® and evaporated to dryness. The residue was recrystallized from a hexanes at −25 °C. Isolated yield: 0.49 g, 79%. For **1**: m.p. (1 atm N_2) 153–156 °C; (0.1 Torr) 154 °C sublime. ^{1}H NMR (300 MHz, C_6D_6, 27 °C) δ 6.22 (s, 1H, Ar–*H*), 3.22 (m, 8H, = C*H*), 2.97 (m, 8H, = C*H*). ^{19}F NMR (282 MHz, C_6D_6) δ −58.8 (s, CF_3). MS *m*/*z* 565 [M^+ − $Rh(C_2H_4)_2$], 752 [M^+ + C_2H_4]; FT-IR (ATR, cm^{-1}): 2962 (w), 2913 (w), 1536 (w), 1511 (w), 1495 (w), 1417 (w), 1344 (w), 1303 (w), 1254 (s), 1205 (w), 1107 (vs), 1017 (m), 1001 (s), 939 (vs), 854 (m), 800 (m). Anal. Found: C, 30.4; H, 2.4; N, 7.9. Calcd: C, 29.8, H, 2.5; N, 7.7%.

$[Rh_2(PMe_3)_4(\mu\text{-}3,5\text{-}(CF_3)(\mu\text{-}Cl)]$ (2). A solution of n-BuLi (0.13 ml, 1.6 M) in C_6H_{14} was added to a solution of 3,5-$(CF_3)_2$PzH (0.21 g, 1.01 mol) in Et_2O (25 ml) at −78 °C. This solution was stirred for 30 minutes and then warmed to room temperature and stirred for 90 minutes. The solution was cannulated into a solution of $[Rh(PMe_3)_2Cl]_2$ (0.587 g, 1.01 mol) in Et_2O at −78 °C. The resulting reaction mixture was warmed to room temperature and stirred overnight forming a white precipitate. The solution was filtered through a short bed of Celite® and evaporated to dryness. The residue was extracted into hexanes and recrystallized at −25 °C to give orange needles. Isolated yield: 0.66 g, 87%. For **2**: m.p. (1 atm N_2) 79–81 °C (dec.). ^{1}H NMR (300 MHz, C_6D_6, 27 °C) δ 7.04 (s, 1H, Ar–*H*), 1.16 (m, 36H, $P(CH_3)_3$). ^{19}F NMR (282 MHz, C_6D_6) δ −57.56 (d, J_{F-P} = 4 Hz); ^{31}P{H} NMR (243 MHz, C_6D_6) δ 2.37 (d, J_{Rh-P} = 167 Hz), 2.11 (d, J_{Rh-P} = 167 Hz), 1.68 (dq, J_{Rh-P} = 204 Hz, $^5J_{P-F}$ = 4 Hz), 1.416 (dq, J_{Rh-P} = 204 Hz, $^5J_{P-F}$ = 4 Hz); MS *m*/*z*: 545 [M^+ − Pz], 672 [M^+ − PMe_3]; FT-IR (ATR, cm^{-1}): 2921 (w), 1537 (w), 1495 (w), 1371 (w), 1295 (m), 1261 (s), 1213 (m), 1118 (vs), 1018 (m), 945 (vs), 855 (m), 802 (w), 744 (m). Anal. Found: C, 27.1; H,4.8; N, 3.7. Calcd: C, 27.3; H, 5.0; N, 3.7%.

$[Rh(PMe_3)_3(\mu\text{-}3,5\text{-}(CF_3)_2Pz)]$ (3). A solution of $[Rh(COD)(\mu\text{-}3,5\text{-}(CF_3)_2Pz)]_2$ (1.01 g, 1.2 mmol) in toluene (75 ml) was stirred at room temperature while PMe_3 (0.87 mL, 8.45 mmol) was added dropwise. The resulting reaction was stirred overnight at room temperature. The solvent was evaporated to dryness under vacuum and the residue was recrystallized in hexanes at −25 °C to give yellow needles. For **3**: m.p. (1 atm N_2) 103–105 °C; (0.1 Torr) 100 °C sublime. Isolated yield: 1.14 g, 89%. ^{1}H NMR (300 MHz, C_6D_6, 27 °C) δ 7.01 (s, 1H, Ar–*H*), 0.89 (dt, 9H, $P(CH_3)_3$), 0.73 (m, 18H, $P(CH_3)_3$). ^{19}F NMR (282 MHz, C_6D_6) δ −58.5 (s, 3F, CF_3), −60.0 (s, 3F, CF_3). ^{31}P{1H} NMR (121 MHz, C_6D_6) δ −0.51 (dt, J_{P-Rh} = 154.1 Hz, J_{P-P} = 47.3 Hz, 1P), −10.21 (dd, J_{P-Rh} = 135.0 Hz, J_{P-P} = 46.5 Hz, 2P). MS *m*/*z*: 331 [M^+ − Pz]; FT-IR (ATR, cm^{-1}): 2962 (w), 2913 (w), 1536 (w), 1511 (w), 1495 (w), 1417 (w), 1344 (w), 1303 (w), 1254 (s), 1205 (w), 1107 (vs), 1017 (m), 1001 (s), 939 (vs), 854 (m), 800 (m). Anal. Found: C, 30.8; H, 5.1; N, 5.1. Calcd: C, 31.5, H, 5.3; N, 5.2%.

$[Rh(PMe_3)_2(\mu\text{-}3,5\text{-}(CF_3)_2Pz)]_2$ (4). A solution of (**1**) (0.169 g, 0.234 mmol) in toluene (40 ml) was added to a stirred solution of (**3**) (0.5 g, 0.936 mmol) in toluene (40 ml) under N_2. Nitrogen was then bubbled through the solution while stirring for 12 hours. The volume was reduced to *ca.* 15 ml and the solution cooled to −25 °C. Yellow crystals formed after **3** days. A second isolation from the filtrate produced inferior product. Isolated

yield: 0.22 g, 34%. For **4**: m.p. (1 atm N_2) 98–100 °C (dec.). ^{1}H NMR (300 MHz, C_6D_6, 27 °C) δ 6.51 (s, 2H, Ar–*H*), 1.07 (pseudo t, J_{P-H} = 3.6 Hz, 36H, P(CH_3)$_3$). ^{19}F NMR (282 MHz, C_6D_6) δ −57.97 (s, 12F, CF_3). ^{31}P{H} NMR (243 MHz, C_6D_6) δ 1.62 (d, J_{Rh-P} = 172.5 Hz). MS *m*/*z*: 916 [M^+], 713 [M^+ − Pz]; FT-IR (ATR, cm^{-1}): 2962 (w), 2910 (vw), 1417 (w), 1299 (s), 1236 (s), 1150 (s), 1121 (s), 1018 (m), 983 (m), 859 (w), 800 (m), 745 (w), 708 (w). Anal. Found: C, 27.1; H, 4.2; N, 5.7. Calcd: C, 27.8; H, 4.6; N, 6.2%.

[Rh(PMe$_3$)$_4$][3,5-(CF$_3$)$_2$Pz] (5). A solution of n-BuLi (1.5 ml, 1.6 M) in C_6H_{14} was added to a solution of 3,5-$(CF_3)_2$PzH (0.493 g, 2.4155 mmol) in Et_2O (40 ml) at −78 °C. This solution was stirred for 30 minutes and then warmed to room temperature and stirred for 90 minutes. The solution was cannulated into a solution of [Rh(PMe$_3$)$_4$]Cl (0.77 g, 2.4155 mmol) in Et_2O (100 ml) at −78 °C. An additional 0.2 mL PMe_3 was added to the solution. The resulting reaction mixture was warmed to room temperature and stirred overnight forming a white precipitate. The solution was filtered through a short bed of Celite® and evaporated to dryness. The residue was recrystallized from a C_6H_{14} with an addition 0.2 mL of PMe_3. Orange needles were formed at −25 °C. For **5**: m.p. 120 °C (1 atm N_2) 99–101 °C sublime to give **4** (0.1 Torr). Isolated yield: 0.94 g, 64%. ^{1}H NMR (300 MHz, C_6D_6, 27 °C) δ 7.04 (s, 1H, Ar–*H*), 0.78 (m, 45H, P(CH_3)$_3$). ^{19}F NMR (282 MHz, C_6D_6) δ −59.2. ^{31}P{H} NMR (121 MHz, C_6D_6) δ −13.1 (br s). MS *m*/*z*: 407 [M^+], 331 [M^+ − PMe_3]; FT-IR (ATR, cm^{-1}): 2974 (w), 2908 (w), 1650 (w, br), 1500 (w), 1423 (w), 1329 (w), 1310 (w), 1289 (w), 1242 (m), 1136 (m), 1105 (s), 1002 (w), 976 (m), 940 (vs), 852 (m), 798 (w), 774 (m), 718 (m); Anal. Found: C, 33.5; H, 5.8; N, 4.8. Calcd: C, 33.5; H, 6.1; N, 4.6.

Single crystal X-ray crystallography

Crystals were mounted on a glass fiber with Paratone N oil. Data collection was carried out on either a Rigaku Saturn CCD (**1–2**) or a Bruker-Nonius Kappa CCD (**3–5**) diffractometer with λ = 0.71073 Å using graphite monochromated Mo Kα radiation. The structures were solved by direct methods. The coordinates of the non-hydrogen atoms were refined anisotropically, while hydrogen atoms were included in the calculation isotropically but not refined. CCDC reference numbers 858611–858615.† Details of crystal data, data collection, and structure refinements are listed in Table 1.

Acknowledgements

The authors would like to thank the Welch Foundation (Grant F-816) and the Petroleum Research Fund, administered by the American Chemical Society (47014-ACS) for financial support. X-ray data was collected on instrumentation purchased with funds from NSF grant # 0741973.

References

1 M. J. Hampden-Smith and T. T. Kodas, *The Chemistry of Metal CVD*, 1994.
2 I. K. Igumenov, N. V. Gelfond, N. B. Morozova and H. Nizard, *Chem. Vap. Deposition*, 2007, **13**, 633–637.
3 E. L. Crane, Y. You, R. G. Nuzzo and G. S. Girolami, *J. Am. Chem. Soc.*, 2000, **122**, 3422–3435.
4 F. Tian and E. F. Chor, *Phys. Status Solidi C*, 2008, **5**, 1953–1955.
5 H. Lee, R. A. Coutu, S. Mall and K. D. Leedy, *J. Micromech. Microeng.*, 2006, **16**, 557–563.
6 G. Hass, *J. Opt. Soc. Am.*, 1982, **72**, 27–39.
7 L. Marot, G. De Temmerman, V. Thommen, D. Mathys and P. Oelhafen, *Surf. Coat. Technol.*, 2008, **202**, 2837–2843.
8 V. Dal Santo, C. Mondelli, V. De Grandi, A. Gallo, S. Recchia, L. Sordelli and R. Psaro, *Appl. Catal., A*, 2008, **346**, 126–133.
9 F. J. Williams, M. S. Tikhov, A. Palermo, N. Macleod and R. M. Lambert, *J. Phys. Chem. B*, 2001, **105**, 2800–2808.
10 R. Kumar and R. J. Puddephatt, *Can. J. Chem.*, 1991, **69**, 108–110.
11 J.-C. Hierso, R. Feurer and P. Kalck, *Coord. Chem. Rev.*, 1998, **178–180**, 1811–1834.
12 (*a*) K. J. Park and G. N. Parsons, *Appl. Phys. Lett.*, 2006, **89**, 043111–043113; (*b*) T. Aaltonen, M. Ritala and M. Leskela, *Electrochem. Solid-State Lett.*, 2005, **8**, C99–C101; (*c*) J. Hamalainen, F. Munnik, M. Ritala and M. Leskela, *J. Electrochem. Soc.*, 2009, **156**, D418–D423; (*d*) S. D. Elliott, *Langmuir*, 2010, **26**, 9179–9182.
13 (*a*) Z. Wang, C. D. Abernethy, A. H. Cowley, J. N. Jones, R. A. Jones, C. L. B. Macdonald and L. Zhang, *J. Organomet. Chem.*, 2003, **666**, 35–42; (*b*) W. J. McCarty, X-P. Yang, L. J. DePue Anderson and R. A. Jones, *Dalton Trans.*, 2012, **41**, 173–179.
14 Y. Chi, H.-L. Yu, W.-L. Ching, C.-S. Liu, Y.-L. Chen, T.-Y. Chou, S.-M. Peng and G.-H. Lee, *J. Mater. Chem.*, 2002, **12**, 1363–1369.
15 (*a*) Y. Chi, E. Lay, T.-Y. Chou, Y.-H. Song and A. J. Carty, *Chem. Vap. Deposition*, 2005, **11**, 206–212; (*b*) O. M. El-Kadri, M. J. Heeg and C. H. Winter, *Dalton Trans.*, 2006, 1943–1953.
16 C. Tejel, J. M. Villoro, M. A. Ciriano, J. A. Lopez, E. Eguizabal, F. J. Lahoz, V. I. Bakhmutov and L. A. Oro, *Organometallics*, 1996, **15**, 2967–2978.
17 G. A. Ardizzoia, S. Brenna, S. Cenini, G. LaMonica, N. Masciocchi and A. Maspero, *J. Mol. Catal. A: Chem.*, 2003, **204–205**, 333–340.
18 L. A. Oro, M. T. Pinillos, A. Tiripicchio and M. Tiripicchio-Camellini, *Inorg. Chim. Acta*, 1985, **99**, L13–L14.
19 C. Tejel, M. A. Ciriano, J. A. López, F. J. Lahoz and L. A. Oro, *Angew. Chem., Int. Ed.*, 1998, **37**, 1542–1545.
20 H. Schumann, G. Cielusek, S. Jurgis, E. Hahn, J. Pickardt, J. Blum, Y. Sasson and A. Zoran, *Chem. Ber.*, 1984, **117**, 2825–2838.
21 A. M. Arif, R. A. Jones, M. H. Seeberger, B. R. Whittlesey and T. C. Wright, *Inorg. Chem.*, 1986, **25**, 3943–3949.
22 B. M. Louie, S. J. Rettig, A. Storr and J. Trotter, *Can. J. Chem.*, 1985, **63**, 688–691.
23 G. Aullon, G. Ujaque, A. Lledos, S. Alvarez and P. Alemany, *Inorg. Chem.*, 1998, **37**, 804–813.
24 R. A. Jones, F. M. Real, G. Wilkinson, A. M. R. Galas, M. B. Hursthouse and K. M. A. Malik, *J. Chem. Soc., Dalton Trans.*, 1980, 511–518.
25 K. Osakada, K. Hataya and T. Yamamoto, *Inorg. Chem.*, 1993, **32**, 2360–2365.
26 S. E. Kegley, C. J. Schaverien, J. H. Freudenberger, R. G. Bergman, S. P. Nolan and C. D. Hoff, *J. Am. Chem. Soc.*, 1987, **109**, 6563–6565.
27 B. M. Louie, S. J. Rettig, A. Storr and J. Trotter, *Can. J. Chem.*, 1984, **62**, 1057–1067.
28 L. M. Haines, *Inorg. Chem.*, 1971, **10**, 1685–1692.
29 K. Burgess, W. A. Van der Donk, S. A. Westcott, T. B. Marder, R. T. Baker and J. C. Calabrese, *J. Am. Chem. Soc.*, 1992, **114**, 9350–9359.
30 O. Blum, J. C. Calabrese, F. Frolow and D. Milstein, *Inorg. Chim. Acta*, 1990, **174**, 149–151.
31 J. H. Rivers and R. A. Jones, *Chem. Commun.*, 2010, **46**, 4300–4302.
32 J. Häglund, A. Fernández Guillermet, G. Grimvall and M. Körling, *Phys. Rev. A*, 1993, **48**, 11685.
33 M. Zumbusch, *Z. Anorg. Allg. Chem.*, 1940, **243**, 322–329.
34 J. Shin, A. Waheed, W. A. Winkenwerder, H.-W. Kim, K. Agapiou, R. A. Jones, G. S. Hwang and J. G. Ekerdt, *Thin Solid Films*, 2007, **515**, 5298–5307.
35 O. Renn, L. M. Venanzi, A. Marteletti and V. Gramlich, *Helv. Chim. Acta*, 1995, **78**, 993–1000.
36 K. Wang, M. E. Goldman, T. J. Emge and A. S. Goldman, *J. Organomet. Chem.*, 1996, **518**, 55–68.
37 R. T. Price, R. A. Andersen and E. L. Muetterties, *J. Organomet. Chem.*, 1989, **376**, 407–417.
38 R. J. Angelici, *Inorg. Synth.*, 1990, **28**, 86–90.

